

## FABRICATION AND OPTICAL PROPERTIES OF WELL-ALIGNED ZnO NANORODS ON SAPPHIRE PREPARED BY CHEMICAL BATH DEPOSITION

GUOZHI JIA\*, YUNFENG WANG<sup>a</sup>, JIANGHONG YAO<sup>a</sup>

*Tianjin Institute of Urban Construction, Tianjin 300384, P. R. China*

*<sup>a</sup>The Key Lab of Advanced Technique and Fabrication for Weak-Light Nonlinear Photonics Materials, Ministry of Education, TEDA Applied Physics School, Nankai University, Tianjin 300475, P. R. China*

Vertically well-aligned ZnO nanorods arrays were synthesized on sapphire substrates by combining sol-gel method and chemical bath deposition (CBD). The thin ZnO seed layer was coated on sapphire using sol-gel method to control the density and orientation of ZnO nanorods. The structural and morphological properties were characterized by X-ray diffraction spectrometer (XRD) and scanning electron microscopy (SEM) respectively. It demonstrated that the ZnO nanorods were hexagonal wurtzite structure and had good crystallinity. Well-aligned and evenly distributed ZnO nanorods in a large scale were obtained, all the ZnO nanorods were preferentially oriented along the c-axis (002) and grown vertically to the substrates. Combining with the Raman scattering and the room temperature photoluminescence (PL), the optical properties are thoroughly studied. At the same time, SEM shows that there are several adjacent rods combine to form aggregation structure, the detail growth mechanism of ZnO nanorods and the new structure is further analyzed.

(Received December 5, 2011; Accepted February 24, 2012)

*Keyword:* ZnO nanorods; Chemical bath deposition; Optical properties

### 1. Introduction

Zinc oxide is one of the most important semiconducting materials due to its wide band gap energy of 3.37eV and large exciton binding energy of 60 meV at room temperature. Kinds of morphologies of ZnO crystals including nanoparticles, nanorods, nanoflower, nanopins have been successfully prepared by various growth technology. Recently, well-aligned ZnO nanowire or nanorods have received an extensive attention because of its potential application in photonic, electronic, optoelectronic and electrochemical nanodevices, such as solar cells [1], laser diodes [2], light emitting diodes [3, 4], gas sensor [5] and so on. Various methods have been reported to prepare well-aligned ZnO nanorod arrays involve aqueous solution method, metal organic chemical vapor deposition, template method and so forth [6-8]. Zhao et al [9] claimed that the size of ZnO nanorods has important influence on the optical properties, so it is essential to thoroughly understand the growth mechanism of ZnO nanorods and take a method to realize their controllable growth.

Among all the methods of preparing ZnO nanorods, chemical bath deposition is more attractive because of its excellent characteristics. It is simple, cost-effective, can be controlled easily and be carried out at low temperature, in addition, chemical bath deposition has become a perfect candidate for large-scale production of nanostructure materials. Jia et al [10] studied the influence of the growth parameters on the morphological of ZnO nanostructure grown by chemical bath deposition. Hamada et al [11] successfully prepared single-crystalline ZnO films on ZnO-buffered a-plane sapphire by chemical bath deposition and a reciprocal space map indicated that the lattice parameters of the ZnO film were very close to the wurtzite-type ZnO. In addition, it is well known that substrate materials are very important for the fabrication of photoelectric

---

\* Corresponding author: dip-coating@163.com

devices. Among all the substrate materials, sapphire substrate has its unique advantages, such as mature production technology, high-crystalline perfection and high stability, especially, ZnO can be prepared epitaxially on the sapphire and has a good flatness, which is beneficial to the production of the photoelectric devices.

In this paper, vertically well-aligned ZnO nanorods arrays on sapphire were prepared by chemical bath deposition. The thin ZnO seed-layer was deposited on the sapphire substrate to control the density and orientation of ZnO nanorods. The structural and optical properties of as-grown ZnO nanorods on sapphire were investigated by XRD, PL and Raman spectrum. As aggregated nanorods had grown, thus the growth mechanism of nanorods and the new structure were further thoroughly analyzed.

## 2. Experiments

All chemicals used in this experiment, such as zinc acetate dihydrate  $\text{Zn}(\text{Ac})_2 \cdot 2\text{H}_2\text{O}$ , hexamethylenetetramine ( $\text{C}_6\text{H}_{12}\text{N}_4$ ), 2-methoxyethanol, diethanol amine (DEA) are analytical reagents and used as purchased without further purification. The synthetic process of the well-aligned ZnO nanorods arrays at low temperature involves two-step chemical solution method.

The first step was coating the ZnO seed on sapphire substrate by a sol-gel method. The detail was as follows: 32.925g  $\text{Zn}(\text{CH}_3\text{COO})_2 \cdot 2\text{H}_2\text{O}$  was dissolved into the 185.61 mL of 2-methoxyethanol under mild magnet stirring and then 14.39 mL of diethanol amine (DEA) was slowly added in the above-mentioned solutions drop by drop as a sol stabilizer. The molar ratio of  $\text{Zn}(\text{Ac})_2 \cdot 2\text{H}_2\text{O}$  and DEA solution was maintained at 1:1. Next, the mixed solution was stirred at 60°C for 2h to form a transparent and homogeneous solution and then aged for 24h before coating process. Subsequently, the sol was coated on the sapphire substrates by pulling method and the pulling rate was set at 5cm/min. After each pulling, the film was dried at 100°C for 10min in order to evaporate the solvent and remove the organic residuals, the above-mentioned process was repeated five times and the resulting film was annealed at 500°C for 1h to form the ZnO film.

The second step was the formation of ZnO nanorods arrays on the as-pretreated sapphire substrate by chemical bath deposition. The equimolar (1:1) mixed solution of zinc acetate dehydrate ( $\text{Zn}(\text{Ac})_2 \cdot 2\text{H}_2\text{O}$ ) and hexamethylenetetramine (HMT) was used. 1.3170g  $\text{Zn}(\text{Ac})_2 \cdot 2\text{H}_2\text{O}$  and 0.8411g  $\text{C}_6\text{H}_{12}\text{N}_4$  were first dissolved into 200mL deionized water using 200mL beaker as container under mild magnet stirring for 5 min at room temperature. The as-pretreated sapphire substrate was immersed and suspended in the mixed solution and the growth of ZnO was carried out by heating the reaction solution from room temperature to 90°C and then stayed for 1.5h without any stirring. The as-grown film was rinsed with deionized water for several times and dried in air at room temperature before characterization.

The structural properties of the as-prepared ZnO nanorods were characterized by Rigaku X-ray diffractometer using Cu-  $\text{K}\alpha$  radiation ( $\lambda = 1.54178 \text{ \AA}$ ). The diffraction angle was scanned from 20° to 80° at the scanning speed of 0.02° per second. The morphology properties were studied by SEM performed on SHIMADZU SS-550 microscopy with 30KV, the room temperature PL spectroscopy was measured using Edinburgh FSP920 fluorescence spectrometer with the Xe lamp as the excitation light source and excitation wavelength was 325nm. The vibrational properties were investigated by Raman spectra recorded on Renishaw Raman spectrometer with 514nm as the excitation wavelength.

## 3. Results and discuss

The scanning electron microscopy (SEM) images of as-prepared ZnO nanorods on sapphire substrate are shown in figure 1(a)-(c). Figure 1a,b exhibit the 45° tilted image of ZnO nanorods, it can be seen that the as-prepared ZnO nanorods are vertically well-aligned to the substrate and evenly distributed in a large scale. The top view of sample is shown in figure c, which indicates that the as-grown ZnO nanorods are hexagonal facets and grow preferentially along the c-axis direction, the diameters of the nanorods are in the range between 50-100nm. The density, size and orientation of as-grown nanarods are mainly depended on the ZnO seed layer [12, 13] which plays a remarkable role in formation of well-aligned and uniformly distributed ZnO nanorods. on one hand, the lattice constants of the ZnO seeds are matching with that of the ZnO nanorods; on the other hand, the ZnO seed-layer provides the nucleation sites for the growth of

ZnO nanorods which thereby decreases the nucleation barrier by decreasing the interface energy and makes the ZnO nanorods easy to grow.[14]

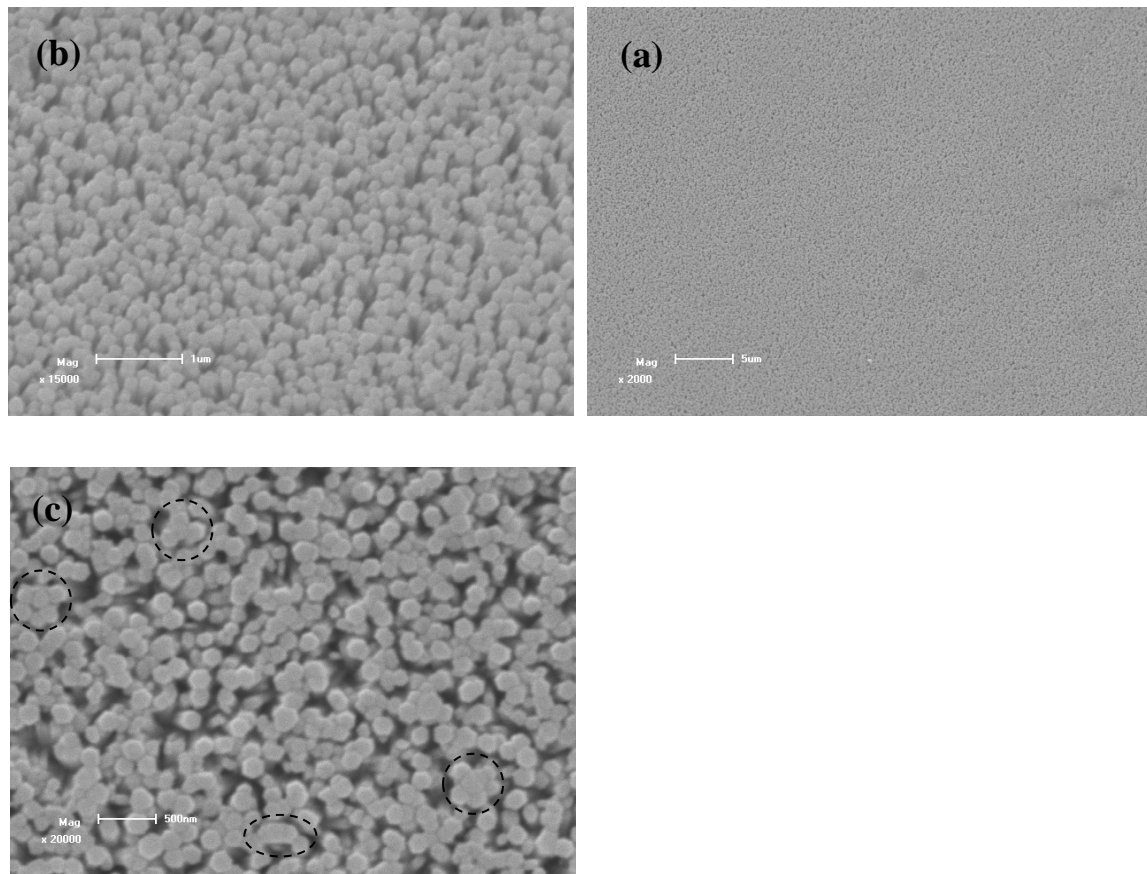
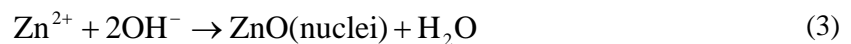
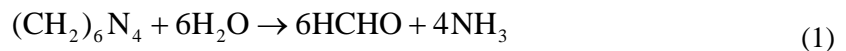


Fig. 1. SEM images of well-aligned ZnO nanorods on sapphire substrate. (a) 45 ° tilted image(scale bar is 5 μm) and (b) corresponding enlarged image(scale bar is 1 μm); (c) top view of the sample (scale bar is 500nm).

The chemical equations involved in the reaction process by CBD are as follows.



As temperature elevates, the decomposition of zinc acetate dihydrate and hexamethylenetetramine accelerates and the concentration of  $\text{Zn}^{2+}$  and  $\text{OH}^-$  increases correspondingly (equ.1 and 2) [15, 16]. When the concentration of the  $\text{Zn}^{2+}$ ,  $\text{OH}^-$  and  $\text{Zn}(\text{OH})_4^{2-}$  reaches a supersaturated degree, the process of rapid nucleation of ZnO starts (equ.3) and ZnO nanostructures begin to generate (equ.4 and 5) in the reactive solution with an appropriate temperature[17]. The formation of nanorods is ascribed to the different growth rates of different directions. The growth rates of the wurtzite hexagonal ZnO crystals are reported to be  $[0001] > [0111] > [0110] > [0111] > [0001]$  under hydrothermal conditions[18]. As the

[0001]facet has the higher surface energy as well as is on the metastable state, according to the thermodynamic equilibrium conditions law, hexagonal ZnO crystals are inclined to grow along the [0001] facet to achieve the surface energy minimization and further result in the formation of nanorods along the c-axis. It is well worth noting that there are lath-like and bundles of ZnO nanorods observed from the top view of ZnO nanorods (figure 1d) indicated using the dotted curves. The formation mechanism of this new structure may be explained as follows. The ZnO nanorods prepared on the sapphire substrate are so compact but the growth space is confined, the continuous longitudinal and transversely growth of nanorods are easy to result in the coalescence of two adjacent nanorods and further form the lath-like and bundles of ZnO nanorods. Another possible mechanism is that nonuniform distribution of the ZnO seed layer due to more pulling times leads to the formation of aggregated nanorods [13], Verma et al demonstrated that the combination of the adjacent nanorods results from the decrease of the lattice mismatch between the ZnO nanorods films and the substrate [19].

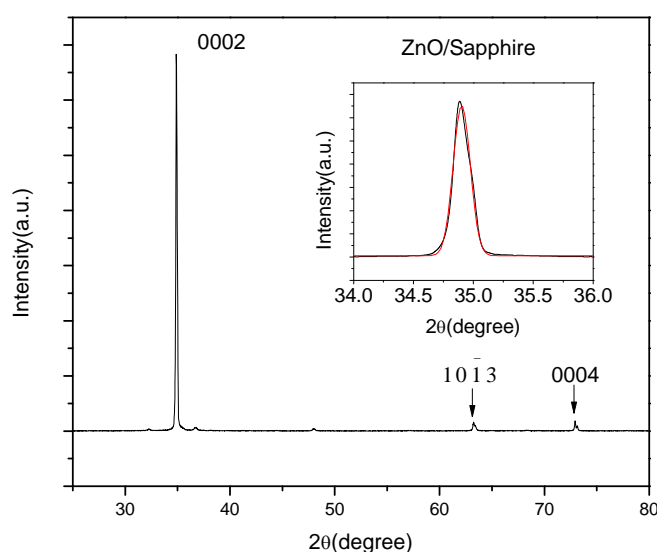


Fig. 2 XRD patterns of as-grown ZnO nanorods on sapphire substrate.

The crystal structure of the as-grown ZnO nanorods was investigated by X-ray diffraction pattern as shown in figure 2. It is observed that the as-grown ZnO nanorods are wurtzite structure, the remarkably sharp peak at  $34.903^\circ$  is assigned to be the [0002] peak of hexagonal wurtzite structure ZnO, the inset pattern is the gauss fitting of [0002] peak, and the full width at half maximum (FWHM) is  $0.1666^\circ$ , the strong and narrow peak indicates that the as-grown samples have good crystallinity and preferentially oriented along the c-axis as well as perpendicular to the substrate surface which is well in agreement with the SEM images. From the analysis of the growth mechanism of vertically well-aligned ZnO nanorods, we can learn that the ZnO seed-layer plays a very important role, however, the interface strain among the substrate, ZnO seed-layer and ZnO nanorods should be taken into consideration. The lattice constants  $a$  and  $c$  of wurtzite structure zinc oxide are calculated according to Bragg's law (1) and the equation (2) which is related with plane spacing and Miller indices [20].

$$2d \sin \theta = n\lambda \quad (1)$$

Where  $d$  is the plane spacing,  $n$  is the order of diffraction that usually is 1,  $\lambda$  is X-ray wavelength.

$$\frac{1}{d_{(hkl)}^2} = \frac{4}{3} \left( \frac{h^2 + hk + k^2}{a^2} \right) + \frac{l^2}{c^2} \quad (2)$$

Where  $d$  is the plane spacing,  $h, k, l$  is the Miller indices. Combining the above equations, the calculation results are  $a=0.32212$ ,  $c=0.513918$ . The strain ( $\varepsilon_{zz}$ ) along the  $c$ -axis among the interfaces is obtained from the following relation (3) [21]

$$\varepsilon_{zz} = (c - c_0) / c_0 \times 100\% \quad (3)$$

Where  $c$  is the calculation value of lattice constants according to the X-ray diffraction pattern while  $c_0$  is the unstrained lattice constant of standard wurtzite structure ZnO. The calculated strain value is  $-1.28\%$ , which indicates that the strain among the substrate, ZnO seed-layer and the ZnO nanorods is the compressive strain due to the strain value  $\varepsilon_{zz}$  is negative, corresponding to the smaller lattice constants than the standard wurtzite structure ZnO (JCPDS Card File No. 36-1451,  $a=0.3249\text{nm}$  and  $c=0.5206\text{nm}$ ).

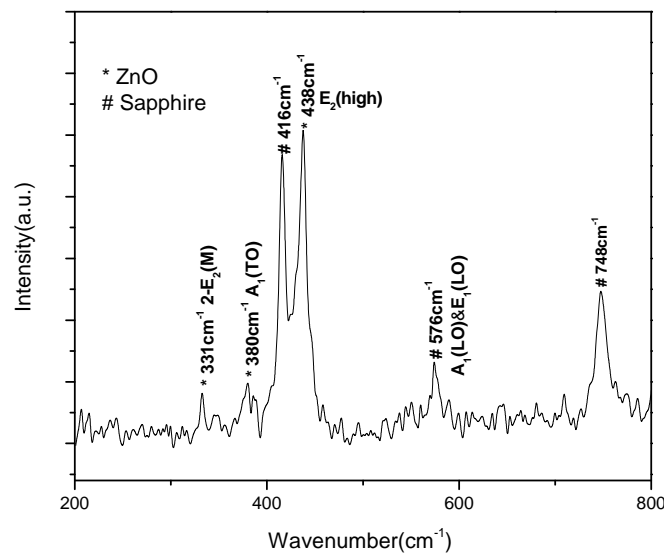


Fig. 3 Raman optical spectra of ZnO nanorods on sapphire by chemical bath deposition.

Hexagonal wurtzite structure ZnO belongs to the space group  $C_{6v}^4$ , Group theory demonstrates that single-crystalline ZnO has eight sets of optical phonon modes at  $\Gamma$  point of the Brillouin zone, summarized as  $A_1 + E_1 + 2E_2 + 2B_1$ , where  $A_1, E_1$  and  $E_2$  modes are Raman active phonons while  $A_1$  and  $E_1$  modes are also infrared active,  $B_1$  (low) and  $B_1$  (high) modes are usually silent. What's more,  $A_1$  and  $E_1$  modes belong to polar symmetries and are split into longitudinal (LO) and transverse (TO) optical components respectively [20, 22]. Figure 3 shows the Raman optical spectra of as-synthesized ZnO nanorods. The remarkable  $E_2$  (high) mode located at  $438\text{cm}^{-1}$  indicates the characteristic of wurtzite structure ZnO. The weak scattering peaks at  $380\text{cm}^{-1}$  and  $576\text{cm}^{-1}$  correspond to  $A_1$  (TO) and  $A_1$  (LO) &  $E_1$  (LO), respectively, which are related to intrinsic defects such as oxygen vacancy, zinc interstitial and so on [23], the peak at  $331\text{cm}^{-1}$  is the second-order Raman scattering peak. The intensity of those peaks is much weaker than that of the  $E_2$  modes, suggesting that ZnO nanorods prepared by chemical bath deposition with the assistance of ZnO seed-layer have small defects. The scattering peaks located at  $416\text{cm}^{-1}$  and  $748\text{cm}^{-1}$  are also observed, associated with the vibrational properties of sapphire [24].

$E_2$  (high) is sensitive to the strain and the frequency shift of  $E_2$  (high) peak results from

the strain variation[24]. By contrast to the  $437\text{cm}^{-1}$  of the bulk ZnO, the  $E_2$ (high) peak of ZnO nanorods prepared in our experiment has slightly blueshift, indicating there are compressive strain [25] among the substrates, ZnO seed-layer and ZnO nanorods, the result is in good accordance with the XRD data analysis in which the strain value is negative.

Fig. 4 shows the room temperature photoluminescence (PL) spectra of as-grown ZnO nanorods on sapphire carried out with 325nm as the excitation source. The near-band-edge (NBE) emission, ranging from 380nm to 430nm and the central value is located at 395nm (3.14eV), is usually ascribed to the radiative recombination of ZnO free excitons [26]. It is well known that the low temperature hydrothermal methods of preparing the ZnO crystalline are very easy to introduce the defects such as oxygen vacancy, zinc vacancy, oxygen interstitial and so forth. The broad visible emission band from 490nm to 800nm as well as central value is around 620nm is closely related to the defects of ZnO. Zhou et al reported that the oxygen vacancy is not the direct reason of yellow-green emission [27] while it may be attributed to the oxygen interstitial defects [28]. In addition, the sharp peak at 471nm results from the xenon lamp spectral line.

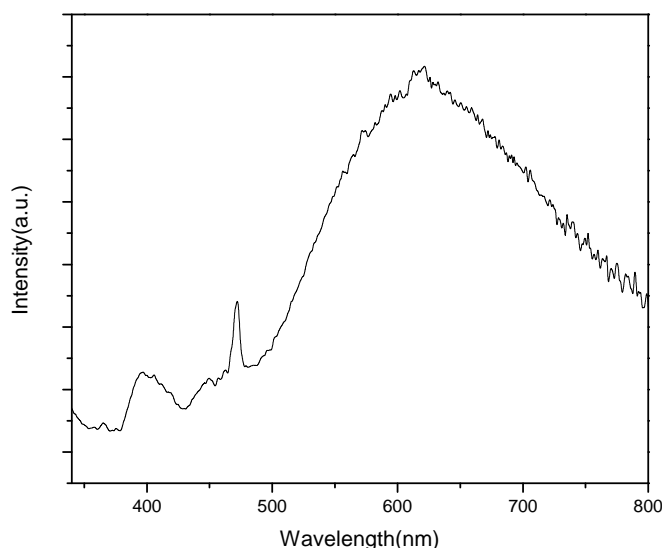


*Fig. 4 Room temperature photoluminescence spectra of as-grown ZnO nanorods on sapphire.*

#### **4. Conclusion**

Vertically well-aligned ZnO nanorods arrays were synthesized on sapphire substrates by chemical bath deposition (CBD). The thin ZnO seed-layer was deposited on the sapphire substrate to control the density and orientation of ZnO nanorods. The structural and optical properties of as-grown ZnO nanorods on sapphire were investigated by XRD, PL and Raman spectrum. The results showed that the ZnO nanorods were hexangular wurtzite structure and had good crystallinity as well as preferentially oriented along the c-axis. There existed small compressive strain among the substrate, ZnO seed-layer and ZnO nanorods and the strain value along the c axis was -1.28%. ZnO seed layer had played an important role in formation of well-aligned ZnO nanorods. In addition, because of spatial limitation, the lath-like and bundles of ZnO nanorods appeared.

#### **Acknowledgements**

This work has been supported in part by the Natural Science Foundation of Tianjin (010JCYBJC04100, 08JCYBJC14800) and the National High Technology Research and Development Program of China (2006AA03Z413).

## Reference

- [1] Hongsith, N.; Choopun, S., *Chiang Mai J. Sci.* **37**(1), 48-54 (2010).
- [2] Liang, H. K.; Yu, S. F.; Yang, H. Y., *Applied Physics Letters*, **96** (10), 101116 (2010).
- [3] Lupan, O.; Pauporte, T.; Viana, B.; Tiginyanu, I. M.; Ursaki, V. V.; Cortes, R., *Applied Materials & Interfaces*, **2**(7), 2083–2090 (2010).
- [4] Guo, Z.; Zhang, H.; Zhao, D. X.; Liu, Y. C.; Yao, B.; Li, B. H.; Zhang, Z. Z.; Shen, D. Z., *Applied Physics Letters*, **97**(17), 173508 (2010).
- [5] Sucheck, M.; Christoulakis, S.; Moschovis, K.; Katsarakis, N.; Kiriakidis, G., *Thin Solid Films*, **515**(2), 551 (2006).
- [6] Le, H. Q.; Chua, S. J.; Koh, Y. W.; Loh, K. P.; Chen, Z.; Thompson, C. V.; Fitzgerald, E. A., *Applied Physics Letters*, **87**(10), 101908 (2005).
- [7] Cong, G. W.; Wei, H. Y.; Zhang, P. F.; Peng, W. Q.; Wu, J. J.; Liu, X. L.; Jiao, C. M.; Hu, W. G.; Zhu, Q. S.; Wang, Z. G., *Applied Physics Letters*, **87**(23), 231903 (2005).
- [8] Sheng, X.; Wei, Y. G.; Kitkham, M.; Liu, J.; Mai, W. J.; Davidovic, D.; Snyder, Robert L.; Wang, Z. L., *Journal of the American Chemical Society*, **130** (45), 14959 (2008).
- [9] Zhao, Q. X.; Yang, L. L.; Willander, M.; Sernelius, B. E.; Holtz, P. O., *Journal of Applied Physics* **104**(7), 073526 (2008).
- [10] Jia, G. Z.; Wang, Y. F.; Yao, J. H., *Journal of Ovonic Research*, **6**(6), 303-307(2010).
- [11] Hamada, T.; Ito, A.; Fujii, E.; Chu, D.; Kato, K.; Masuda, Y., *Journal of Crystal Growth*, **311**(14), 3687–3691 (2009).
- [12] Lee, S. D.; Kim, Y. S.; Yi, M. S.; Choi, J. Y.; Kim, S. W., *Journal of Physical Chemistry C*, **113**(20), 8954–8958 (2009).
- [13] Zhang, H.; Yang, D. R.; Ma, X. Y.; Du, N.; Wu, J. B.; Que, D. L., *Journal of Physical Chemistry B* **110**(2), 827-830 (2006).
- [14] Qiu, J. J.; Li, X. M.; He, W. Z.; Park, S. J.; Kim, H. K.; Hwang, Y. H.; Lee, J. H.; Kim, Y. D., *Nanotechnology* **20** (15), 155603 (9pp) (2009).
- [15] Ahsanulhaq, Q.; Kim, S. H.; Hahn, Y. B., *Journal of Physics and Chemistry of Solids*, **70**(3-4), 627-631 (2009).
- [16] Tang, J.; Yang, X. R., *Materials Letters*, **60** (29-30), 3487-3491 (2006).
- [17] Jang, J. H.; Park, J. H.; Oh, S. G.; *Journal of Ceramic Processing Research*, **10**(6), 783 (2009).
- [18] Umar, A.; Ribeiro, C.; Al-Hajry, A.; Masuda, Y.; Hahn, Y. B., *Journal of Physical Chemistry C*, **113**(33), 14715–14720 (2009).
- [19] Verma, H.; Mukherjee, D.; Witanachchi, S.; Mukherjee, P.; Batzill, M., *Journal of Crystal Growth*, **312** (12-13), 2012–2018 (2010).
- [20] Lupan, O.; Chow, L.; Ono, L. K.; Cuenya, B. R.; Guangyu Chai, Khallaf, H.; Park, S.; Schulte, A., *Journal of Physical Chemistry C*, **114**, 12401–12408 (2010).
- [21] Ghosh, R.; Basak, D.; Fujihara S., *Journal of Applied Physics*, **96**(5), 2689 (2004).
- [22] Zhang, Y.; Jia, H. B.; Wang, R. M.; Chen, C. P.; Luo, X. H.; Yu, D. P.; Lee, C., *Applied Physics Letters*, **83** (22), 4631 (2003).
- [23] Xu, C. X.; Zhu, G. P.; Li, X.; Yang, Y.; Tan, S. T.; Sun, X. W.; Lincoln, C.; Smith, T. A., *Journal of Applied Physics* **103** (9), 094303 (2008).
- [24] Cong, G. W.; Wei, H. Y.; Zhang, P. F.; Peng, W. Q.; Wu, J. J.; Liu, X. L.; Jiao, C. M.; Hu, W. G.; Zhu, Q. S.; Wang, Z. G., *Applied Physics Letters*, **87**(23), 231903 (2005).
- [25] Lo, S. S.; Huang, D., *Langmuir*, **26**(9), 6762–6766 (2010).
- [26] Feng, Y.; Zhou, Y. X.; Liu, Y. Q.; Zhang, G. B.; Zhang, X. Y., *Journal of Luminescence*, **119-120**, 233-236 (2006).
- [27] Zhou, H. L.; Shao, P. G.; Chua, S. J.; Kan, J. A. van; Bettiol, A. A.; Osipowicz, T.; Ooi, K. F.; Goh, G. K. L.; Watt, F., *Crystal Growth and Design*, **8** (12), 4445-4448 (2008).
- [28] Wang, Y. G.; Lau, S. P.; Lee, H. W.; Yu, S. F.; Tay, B. K.; Zhang, X. H.; Hng, H. H., *Journal of Applied Physics*, **94**(1), 354 – 358 (2003).